Graphite-coated ZnO nanosheets as high-capacity, highly stable, and binder-free anodes for lithium-ion batteries

Eliana Quartarone[*,a], Valentina Dall'Asta[a], Alessandro Resmini[a], Cristina Tealdi[a], Ilenia Giuseppina Tredici[a], Umberto Anselmi Tamburini[a], Piercarlo Mustarelli[a]*

[a] Dept. of Chemistry, Division of Physical Chemistry, and INSTM, University of Pavia

Via Taramelli 16, 27100 Pavia, Italy

*E-mail: eliana.quartarone@unipv.it

Abstract

ZnO is one of the materials of choice as anode for lithium batteries, due to its high theoretical capacity, natural abundance, low toxicity, and low cost. At present, however, its industrial exploitation is impeded by massive capacity fading, and by cycling instability due to the drastic volume expansions during the electrochemical lithiation/delithiation process. Herein, we present a novel graphite coated-ZnO anode for LiBs based on films of nanosheets, coated with graphite. The electrode is obtained by a simple and inexpensive solution hydrothermal synthesis, whereas the graphite is deposited by thermal evaporation, which is easier to perform than a wet chemistry technique. Our approach leads to a substantial increase of the permanent specific capacity, obtaining values of 600 $mAhg^{-1}$ after 100 cycles at a high specific current of 1 Ag^{-1}. This represents the best performance for long-cycled, ZnO-based anodes obtained so far. Such result derives from the peculiar porous structure of the nanosheets film (pore diameter <1 nm), as well as by the graphite coating that works as a dimensional buffer and preserves its

morphology during cycling. This appears a very promising strategy for designing more stable ZnO-based anodes for Li batteries and microbatteries.

Keywords: ZnO, nanosheets, binder-free anodes, Li Storage, Li Batteries

1. Introduction.

Lithium ion batteries (LIB) have been widely studied for several decades due to their excellent advantages in terms of high voltage, recyclable and long using lifetime. The need to replace Li metal as the anode in LIB because of the formation of dendrites upon cycling represents a major challenge [1,2]. In fact, the dendrites are electrically isolated but highly chemically active, resulting in a dramatic loss of energy density as well as in the appearance of safety problems, such as thermal runaway, internal short circuits and consequent explosions can be experienced [2]. The research is then directed towards alternative materials, resulting more stable during the charge/discharge cycling, but without any reduction in lightness, power and energy densities [2,3]. Recent advances in nanotechnology allowed the design of innovative nanostructures of different metals or metal oxides, which can be of great interest in lithium storage because of their unique properties, such as high surface area, short Li^+ diffusion path lengths and high electron transportation rate [4,5]. Carbon- and silicon-based systems, alloys, transition metal oxides, obtained as mono- (1D) and two-dimensional (2D) nanostructures, e.g. nanorods, assembled nanoparticles, nanotubes, nanosheets, nanoflowers, nanowires, were proposed as anodes for LIB and discussed in terms of their relationships among particles size, surface area and morphology and the electrochemical performances [4, 5]. Moreover, most of these nanoarchitectures may be easily grown on conductive metal substrates as nanostructured films and directly used as binder-free electrodes, contrary to the conventional anode materials for which proper ink preparation is required. The array geometries offer wide potential in terms of easier electrode processing, faster ion and electron transport, wider electrode/electrolyte interface and, which is of paramount importance, better accommodation of the strains deriving from lithium (de)/intercalation (or (de)/alloying reactions in case of alloys) [6].

In this frame, ZnO has gained a relevant attention during the most recent years. The electrochemical lithiation of ZnO is considered to take place according to a two-steps

mechanism [7], involving the initial reduction of zinc oxide to metallic zinc accompanied by the formation of amorphous Li_2O (Eq. 1), followed by the alloying of zinc with up to one lithium (Eq. 2), so resulting in an overall specific capacity, C_s, of 987 mAh g^{-1}, given by

$$ZnO + 2Li^+ + 2e^- \rightarrow Zn^0 + Li_2O \qquad C_s = 658 \text{ mAh } g^{-1} \qquad (1)$$

$$Zn^0 + Li^+ + e^- \rightarrow Zn= + LiZn \qquad C_s = 329 \text{ mAh } g^{-1} \qquad (2)$$

Whereas reaction (1) is fully reversible, the reversibility of reaction (2) is low, although not negligible [8].

ZnO can be synthesized following a number of different nanoarchitectures, both as powder and thin films, and also tested in binder-free anodes for LIB [4]. However, ZnO suffers of poor kinetics and drastic volume changes during cycling, resulting in a large capacity fading during the initial cycles and reduced life cycle. Several attempts to improve the ZnO electrochemical performances were recently carried out. Doping with transition metals, like Co or Fe, resulted in a remarkable enhancement of the specific capacity of the powder-based anode with respect to the undoped ZnO under similar testing conditions (e.g. 670 $mAhg^{-1}$ vs. 260 $mAhg^{-1}$ at a specific current of 0.095 Ag^{-1}) [7]. The modulation of the structure from bulk to nanoarchitectures such as nanorods [9-12], nanotubes [13], needles and nanowires [14, 15], nanosheets [16-19], resulted in an enhancement of the specific capacity of about two times with respect to that of the bulk, with values ranging between 500 and 300 $mAhg^{-1}$ in the specific current range 0.1-0.5 Ag^{-1}.

Finally, the addition of carbon and carbon-based materials may increase the performances of ZnO anodes in terms of cycling stability and rate capability, as confirmed by some recent papers on ZnO nanoparticles or other nanostructures carbon-coated by means of wet-chemistry processes (e.g. via carbothermal synthesis, graphene-based composites, glucose solution or bottom-up assembly routes) [20-24]. Recently, MOF-based ZnO@ZnO quantum dots/C nanorods arrays were growth on carbon cloth, which showed good properties in terms of capacity retention at relatively high currents [25]. Despite of numerous attempts to overcome

the limits shown by ZnO-based anodes, drastic morphology degradation phenomena may be observed both in bulk powder and in nanostructures, such as nanoamorphization, nanocracking or disordering of the porous network, which still prevent the application of ZnO as a battery electrode [8, 26].

Here, we reported the excellent electrochemical performances of films based on ZnO nanosheets (NS) coated with a graphite layer, as binder-free anodes for lithium batteries. In particular, our work pointed towards the deposition of high-surface area films of ZnO nanosheets, as well as the stabilization of the nanosheets morphology against the intrinsic volume expansion induced by ZnO (de)alloying upon cycling. Our overall strategy included: i) obtaining a unique nanosheets morphology, optimizing the synthetic route so that low-cost and safe chemicals as well as simple procedures are employed and no seed-layers are needed, ii) producing a uniform film of NS presenting controlled overall thickness, and iii) introducing a graphite layers with different thickness as a buffering agent by means of physical procedures (e.g. thermal evaporation), which are easier, faster and cheaper than the wet chemistry approach usually reported in the literature. The results of anodes based on graphite-coated ZnO NS are compared with the uncoated ones.

2. Experimental Section

2.1 Synthesis of ZnO nanosheets and anode preparation.

Stainless steel disks (diameter: 10 mm, thickness: 0.5 mm, AISI 304) were used both as substrate for the ZnO nanostructure and as current collector. After deep mechanical polishing and subsequent washing with acetone, the disks were covered with a platinum layer (200 nm), in order to protect them from the reactants chosen for the hydrothermal synthesis and to improve the oxide adhesion.

The ZnO nanosheets were synthesized by hydrothermal treatment at low temperature and pressure. An aqueous diluted solution of zinc nitrate hexahydrate, sodium citrate sesquihydrate and hexamethyleneamine was first prepared in a 100 mL Duran GL45 glass laboratory bottle. Then the substrates, each one fastened to square (2.5cm x 2.5cm) microscope slide glass with PTFE-tape, were vertically immersed in the solution and the bottle sealed with a PTFE cap. The hydrothermal synthesis was carried out at 60 °C for 6 hours. The films of hybrid nanosheets grown on the SS disks were subsequently rinsed with distilled water and dried at room temperature for 24 hours. The films were finally annealed in static air at 350 °C for 1 hour with a heating rate of 5 °C/min. Graphite coating of ZnO NS was subsequently carried out by means of a thermal evaporation process (Cressington 208carbon – high vacuum carbon coater). Two different graphite layer thicknesses, namely 110 Å (G_{110}-NS) and 350 Å (G_{350}-NS), were obtained by modulating the thermal evaporation conditions: chamber pressure $<10^{-4}$mbar; voltage setting=5.5V; deposition times were 10s and 30s to prepare G_{110}-NS and G_{350}-NS, respectively.

2.2 Characterization.

X-ray diffraction patterns (XRD) of the annealed ZnO nanosheets deposited onto Pt coated stainless steel were acquired in Bragg-Brentano geometry on a Bruker D8 Advance diffractometer with Cu Kα radiation in the 20-80° 2θ range with step size of 0.02° and fixed counting time of 20 seconds per step.

HiRes-SEM analysis was carried out by means of a Tescan Mira 3 microscope. The image analysis to estimate the nanosheets dimensions was performed thanks to ImageJ software [27]. The thickness of the NS was determined by using a KLA Tenkor P6 profiler (KLA Tencor, Milpitas CA). To this aim, large 2D profiles were collected at the scan rate of 50 μm s^{-1} and sampling rate of 50 Hz. A diamond stylus with a tip radius of 2 μm was used by applying a

force of 0.5 mg. The images were analyzed and processed by means of the Apex 3D software (KLA Tencor). 3D scans were carried out by collecting at least 150 profiles with a distance of 10 μm between the rows.

The electrochemical tests were performed using a Swagelok-type cell where the ZnO NS film, deposited on the SS substrate, was directly used as binder-free anode, Li as both counter-electrode and the reference electrode and a glass-wool (Whatman GF/A) disc was used as the separator. The liquid electrolyte was a standard solution of EC/DEC (1/1 v/v)- $LiPF_6$ (1 M) (Merck). Each semi-cell was assembled in a dry-box under Argon atmosphere (H_2O, O_2< 1 ppm). The cyclic voltammetry (CV) was performed by using an Electrochemical Interface (Solartron 1287) at a scan rate of 0.1 mV/sec in the potential range 0 – 3.0V. The galvanostatic charge-discharge cycling tests were carried out using an Arbin battery cycler (model BT-2000). The cells were charged and discharged at 1.0 Ag^{-1} for 100 cycles in the range from 0 – 3.0 V. All the cells were tested at ambient temperature, without any thermal control, in order to investigate their behaviour as far as possible under real conditions.

3. Results and discussion

Films of ZnO NS deposited directly onto stainless steel substrates (SS) were obtained using a two-steps process. The first step involved the solution-based deposition of a precursors of ZnO NS represented by Zn-based hybrid organic-inorganic NS. This precursor was subsequently converted into ZnO by thermal degradation. Solution-based deposition of NS hybrid thin films was carried out in water solvent, making use of low-cost and safe chemicals such as zinc nitrate, sodium citrate dibasic and hexamethylenetetramine (HMT). A key-feature of this solution-based process is represented by its ability to produce the deposition of NS thin films directly onto generic substrates (e.g. glass, silicon, steel, kapton, etc.) without any need for a specific seed-layer. Films of hybrid NS deposited through such solution-based process are highly

uniform and can be easily obtained over areas several square centimeters large. Thermal conversion in air at temperature in the range 250-350 °C fully degrades hybrid NS into ZnO ones. The formation of micropores (diameter <1 nm) within the sheet's architecture, due to the nucleation of small nanoparticles of ZnO, may increase even further the exposed surface area of the final ZnO NS films.

The success of synthesis of typical ZnO NS was confirmed by scanning electron microscopy (SEM) and X-ray diffraction (XRD) analyses. Figure 1a-c reports the SEM images of the films, grown on Pt-SS substrate, before and after the coating with graphite. The micrographs show the presence of finely packed nanosheets, each of them constituted by nanoparticles well interconnected to form a microporous 2D network. The estimated size of the nanoparticles is about 15 nm, whereas the NS width and length range between 0.8 and 1.5 μm, as determined by means of profilometry scans, an example of which is reported in the Supplementary Material (see Figure S1). The morphology of the NS does not change in presence of graphite coating, either in terms of system morphology or microporosity. However, in the case of G_{350}-NS, the thickening of the NS is evident.

Figure 2 shows the XRD pattern of the ZnO NS without C-coating, deposited onto Pt-coated SS. The films prepared under the conditions used in this study are polycrystalline with wurtzite (hexagonal) structure (JCPDS No. 36- 1451), characterized by a strong preferential orientation along the *c* direction, as indicated by the relative intensity of the (0 0 2) reflection compared to the (1 0 0) and (1 0 1) ones. Preferential growth of ZnO polycrystalline film along the *c* direction has been frequently observed as a result of different deposition techniques. Depending on the synthetic conditions and/or the nanoarchitecture presented by the ZnO film, the degree of preferential orientation may be a function of the annealing temperature [28-31].

The average crystallite size, evaluated by applying the Scherrer equation to the peak width at half maximum of the (0 0 2) reflection, was found to be approximately 20 nm, in very good agreement with the determination performed on the basis of the SEM images.

The ZnO films grown on Pt-SS substrates were directly used as binder-free anodes of lithium ion cells, and their electrochemical properties were studied by means of cyclic voltammetry and galvanostatic charge-discharge cycling. The uncoated ZnO NS film was compared with the graphite-coated ones in order to evaluate the role of the carbon layer on the electrochemical performances. Figure 3 shows the cyclic voltammograms, collected between 0 and 3.0 V at the scan rate of 0.1 mV s^{-1} of NS- (a), G_{110}-NS- (b) and G_{350}-NS- (c) based cells. The first cathodic scan of uncoated ZnO NS shows an intense peak at 0.42 V, that is mainly due to the growth of the solid electrolyte interface (SEI) and of a passivation layer coming from the partial decomposition of organic carbonate solvents and Li salt, constituting the liquid electrolyte [19]. The phenomena in the range 0.6-0.8V and the broad peak at 1.5V are likely due the reduction of ZnO to Zn, and to the formation of the Zn-Li alloy, respectively [18]. In the anodic scan several peaks are observed between 0 and 0.7 V, that can be associated to the delithiation process of the Zn-Li alloy to give metal Zn. As reported in the literature, the de-alloying process occurs through different intermediates, such as LiZn, Li_2Zn_3, $LiZn_2$ and Li_2Zn_5 [17]. Finally, the broad signal peaked at 1.34 V is related to the formation of ZnO from the redox reaction between Zn^0 and Li_2O [12]. After the 1st cycle, the plots became almost identical in terms of shape and peaks position, so indicating a good reversibility of the redox processes. The only difference concerns the intensity of the peak at 0.42 V, which undergoes a reduction in the subsequent cycles as already reported in the literature [19]. Similar voltammograms were collected for the carbon-coated ZnO NS films, suggesting that, even in case of the thicker graphite layer, the presence of the coating does not alter the electrochemical behaviour of the ZnO nanosheets.

The lithiation/delithiation process was further investigated by means of galvanostatic discharge-charge cycles on semi-cells based on NS films as binder-free anodes. The cells were cycled at ambient temperature for 100 times at a constant current density of 1 A g^{-1}. The electrode made of uncoated ZnO NS was compared with those based on the coated samples

(G_{110}-ZnO NS and G_{350}-ZnO NS) in order to evaluate the actual role of the graphite in determining the anode performances. Figure 4 reports the galvanostatic charge-discharge profiles of the 1st, 50th, and 100th cycle for all the investigated anodes (a-c), and the corresponding profiles of differential capacity vs. voltage (d-f), which are well comparable with the voltammograms of Figure 3. Interestingly, the anodic parts of the curves (d-f) point out that the irreversible capacity is likely related both to the de-alloying processes and to ZnO formation. Figures 5 and 6 report the cycling performances along all the 100 cycles, and the related coulombic efficiencies, respectively. During the first cycle, the discharge and charge capacities of uncoated ZnO NS electrode are about 1212 $mAhg^{-1}$ and 780 $mAhg^{-1}$, respectively. Bad columbic efficiency of the first cycle is frequently observed for metal oxide anodes, because of the difficult delithiation reaction of Li_2O in absence of catalysts [12]. During the initial 10 cycles the specific capacity rapidly fades to ~600 $mAhg^{-1}$, then approaching 400 $mAhg^{-1}$ upon continuous cycling, with coulombic efficiency near to 100%. In spite of the initial capacity loss, such a value of specific capacity is higher than those typically reported in the literature for ZnO bulk or on similar binder-free ZnO electrodes tested under the same conditions [7, 19]. Bigger capacity fading is generally observed, and specific capacities less than 200 $mAhg^{-1}$ are reported in case of ZnO NS films cycled at the current density of 1 Ag^{-1}. The higher delivered capacity and enhanced cycling performances of our ZnO NS with respect to those reported in literature may be interpreted in terms of higher exposed surface area, which is due to both the nanostructure and to the very small nanoparticles dimensions (<15 nm), resulting from the novel synthesis we described. This produces larger electrode/electrolyte contact area, improved electrical contact and a better strain accommodation.

However, the capacity fading is still relevant, as also evidenced by the corresponding voltage profiles reported in Figure 4a for the 1st, 50th and 100th selected cycles. As already stated, such a rapid fading is due to the change of ZnO morphology, caused by volume expansion undergoing during the electrochemical alloying/de-alloying processes [8, 26]. This structural

evolution becomes evident from the *post-mortem* SEM analysis. Figure 7 shows the SEM images obtained for the ZnO NS film-based electrodes after the galvanostatic cycling (100 cycles) at 1.0 A g^{-1}. By comparing the micrographs of the uncoated ZnO NS electrode before and after the tests, a deep degradation of the material morphology is observed in consequence of the cycling. The nanosheets-based architecture collapses upon cycling, leading to a cracked and porous network of interconnected nanoparticles. The group of Kushima recently discussed similar modifications on ZnO nanowires. By in-situ transmission electron microscopy, the Authors evidenced the formation of glassy nanodomains and nanocracks, induced by the partial alloying upon the first cycle [8]. The porosity evolution of the nanostructure is another important aspect to be considered when it has to do with electrochemical cycling. It was observed, for instance, that pores dimension generally increases upon cycling by a mechanism similar to Ostwald ripening, particularly in presence of high current density. As an example, battery cycles were adopted to generate modulated porous nanostructures in case of ZnO nanoarchitectures and silicon or silver nanowires [26].

Whereas the results for uncoated ZnO NS are already promising in comparison with the literature, a real breakthrough is offered by the graphite coating, in terms of specific capacity, control of volume expansion and the consequent morphological stability. The discharge/charge galvanostatic data, reported in Figure 4 b,c, show capacities in the first cycle of ~ 937 and ~570 $mAhg^{-1}$, respectively, for the anodes based on G_{110}-ZnO NS and 1470 $mAhg^{-1}$ 968 $mAhg^{-1}$ for those based on G_{350}-ZnO NS.

The G_{110}-ZnO anode shows cell performances similar to those of the uncoated anode, except for better cycling stability, with a specific capacity of around 400 $mAhg^{-1}$ at specific current of 1 Ag^{-1}. Remarkably higher values are obtained in presence of a larger amount of graphite. Even if the capacity fading is still present, this is much smaller than in the uncoated film (38% vs. 51%). In addition, good reversibility is obtained upon long-term cycling with a specific capacity exceeding 600 $mAhg^{-1}$ and columbic efficiency ~100% after 100 cycles. This is an excellent

result since, to our knowledge, specific capacities higher than 500 $mAhg^{-1}$ at applied currents greater than 0.5 Ag^{-1} have never been reported for binder-free anodes based on ZnO nanoarchitectures (see table 1). This value is roughly twice that of the graphite itself, which is still the reference material as anode material in lithium batteries. Some beneficial effects of carbon-based coating have been reported in the literature for nanostructured ZnO, doped with transition metals, and ZnO nanorods/reduced graphene oxide composites [7, 21, 23, 24]. The improvement of the specific capacity produced by the graphite coating is likely related to better interconnection of the NS, as well as to the role of graphite itself as active material. However, by means of weight considerations, and by considering the theoretical capacity of graphite and ZnO, we estimated graphite contribution to the overall anode capacity to be less than 3%. Capacity retention, on the other hand, is probably related to a sort of buffering action on volume expansion [7], which preserves the mechanical integrity of the NS films. The beneficial effect of the graphite layer on the NS morphological stability is confirmed by the SEM images of Figure 4. By comparing them with those of the electrodes before the functional tests (Figure 1), we may note that in case of coating with a thicker graphite layer, G_{350}-ZnO NS, the NS morphology appears to be well preserved. In contrast, in case of G_{110}-ZnO NS electrodes, NS suffer evident microstructure degradation, although not severe as in the case of the uncoated ZnO anode. This suggests that a minimum thickness of the graphite layer (higher than 110 Å in our case) is required in order to observe a beneficial effect on the electrochemical performances. On the other hand, an exceedingly thick graphite layer would lead to the loss of the properties offered by the NS microstructure as an active anode component. For this reason, work is in progress to investigate the relationships between the thickness of the graphite coatings and the specific capacity, reversibility and the cycling stability, particularly in the case of high currents, which have been proved to kinetically limit the lithiation/delithiation process [7].

4. Conclusions

Films of ZnO nanosheets both uncoated (ZnO NS), and coated with different amounts of graphite (G_{110}-ZnO NS and G_{350}-ZnO NS), were prepared and tested as binder-free anodes for Li batteries. Films of ZnO NS were deposited directly on conductive and non-specific substrates by a simple solution-based method involving the formation of a Zn-based hybrid organic-inorganic precursor. This method does not require seed-layers and involves only aqueous solvent and low-cost and safe chemicals. Final annealing of the hybrid NS film led to their full conversion into ZnO. The graphite coating was obtained by means of a simple thermal evaporation technique. With respect to the state of the art, some important improvements were obtained:

i) these anode materials shows remarkably higher specific capacity than those discussed in literature for other ZnO systems (both powder or nanostructures). This is due to the unique morphology, characterized by the presence of a particularly extended microporous texture, allowing large space for accommodating the volume changes upon lithiation/delithiation, and by well-interconnected small nanoparticles (<15 nm), which maximizes the film specific surface area and promotes the formation of the LiZn alloy;

ii) graphite layer plays a beneficial role in stabilizing the morphology, does enhance the specific capacity and improves reversible capacity. In the case of the 350Å-thick graphite layer, the ZnO anode shows reduced capacity fading and specific capacity values of ~600 $mAhg^{-1}$ at 1 Ag^{-1} upon 100 cycles. Furthermore, the graphite coating preserves the NS morphology from the degradation caused by the electrochemical reactions.

This outstanding result is unprecedented, and we believe that this optimized combination of nanoarchitectures with a proper buffering agent such as graphite may represent a versatile, low-cost and simple approach to the exploitation of ZnO potential as anode in Li storage.

References.

[1] M. Armand, J.M. Tarascon, Nature, 451 (2008) 652-657.

[2]. K. Xu, Chem. Rev., 104 (2004) 4303-4418.

[3]. V. Etacheri, R. Marom, R. Elazari, G. Salitra, D. Aurbach, Energy Environ. Sci., 4 (2011) 3243-3262.

[4]. J. Liu, X.-W. Liu, Adv. Mater., 24 (2012) 4097-4111.

[5]. P. Roy, S.K. Srivastava, J. Mater. Chem. A, 3 (2015) 2454-2484.

[6]. J. Jiang, Y. Li, J. Liu, X. Huang, Nanoscale, 3 (2011) 45-58.

[7]. D. Bresser, F. Mueller, M. Fiedler, S. Krueger, R. Kloepsch, D. Baither, M. Winter, E. Paillard, S. Passerini, Chem. Mater., 25 (2013) 4977-4985.

[8]. A. Kushima, X.H. Liu, G. Zhu, Z.L. Wang, J.H. Huang, J. Li, Nano Lett., 11 (2011) 4535-4541.

[9]. S., S. Sain, M. Yoshio, T. Kar, N. Gunawardana, S.K. Pradhan, Appl. Surf. Sci., 329 (2015) 206-211.

[10]. H. Wang, Q. Pan, Y. Cheng, J. Zhao, G. Yin, Electrochimica Acta, 54 (2009) 2851-2855.

[11]. X.H., J.B. Wu, Y. Lin, R.Q. Guo, Int. J. Electrochem Sci., 7 (2012) 6611-6621.

[12]. M.-S. Wu, H.-W. Chang, J. Phys. Chem. C., 117 (2013) 2590-2599.

[13]. K.T Park, F. Xia, S.W. Kim, S.B. Kim, T. Song, U. Paik, W.I., J. Phys. Chem. C., 117 (2013) 1037-1043.

[14]. J. Yan, G. Wang, H. Wang, Z. Zhang, X. Ruan, W. Zhao, J. Yun, M. Xu, J. Nanopart. Res., 17 (2015): 52.

[15]. H.-J. Wang, S.-C. Lim, S.-Y. He, H.-Y. Tuan, RCS Adv., 5 (2015) 33392-33399.

[16]. F. Li, L. Yang, G. Xu, H. Xiaoqiang, X. Yang, X. Wei, Z. Ren, G. Shen, G. Han, J. All. Comp., 577 (2013) 663-668.

[17]. J. Liu, Y. Li, X. Huang, G. Li, Z. Li, Adv. Funct. Mater., 18 (2008) 1448-1458.

[18]. X. Wu, S. Li, B. Wang, J. Liu, M.Yu, RSC Adv., 5 (2015) 81341-81347.

[19]. X.H. Huang, X.H. Xia, Y.F. Yuan, F. Zhou, Electrochimica Acta, 56 (2011) 4960-4965.

[20]. Y. Shen, J. Mater. Chem. A, (2015) DOI:10.1039/c5ta01228g.

[21]. J. Wu, C. Chen, Y. Hao, C. Wang, Coll. Surf. A., 468 (2015) 17-21.

[22]. Q. Pan, L. Qin, J. Liu, H. Wang, Electrochimica Acta, 55 (2010) 5780-5785.

[23]. J. Liu, Y. Li, R. Ding, J. Jiang, Y. Hu, X. Ji, Q. Chi, Z. Zhu, X. Huang, J. Phys. Chem. C., 113 (2009) 5336-5339.

[24]. G.Z. Yang, H.W. Song, H. Cui, Y.C. Liu, C.X. Wang, Nano Energy, 2 (2013) 579-585.

[25]. G. Zhang, S. Hou, H. Zhang, W. Zeng, F. Yan, C.C. Li, H. Duan, Advanced Materials, 27 (2015) 2400-2405

[26]. J.W. Choi, J. McDonough, S. Jeong, J.S. Yoo, Nano Lett., 10 (2010) 1409-1413.

[27] W.S. Rasband, J. Image, U.S. National Institutes of Health, Bethesda, MD, USA (1997-2001) http://imagej.nih.gov/ij/

[28]. S. Yamabi, H. Imai, J. Mater. Chem., 12 (2002) 3773-3778.

[29]. J. Demel, J. Plestil, P. Bezdicka, P. Janda, M. Klementov, K. Lang, J. Phys. Chem. C, 115 (2011) 24702-24706.

[30]. M. Mo, J.C. Yu, L. Zhang, S-K A. Li, Adv. Mater., 17 (2005) 756-760.

[31]. A. Resmini, I.G. Tredici, C. Cantalini, L. Giancaterini, F. De Angelis, E. Rondanina, M. Patrini, D. Bajoni, U. Anselmi-Tamburini, J. Mater. Chem. A, 3 (2015) 4568-4577.

[32] X.H. Huang, J.B. Wu, Y. Lin, R.Q. Guo, Int. J. Electrochem. Sci 7 (2012) 6611.

Figure Captions

1. SEM Micrographs (Mag. 200 kx) of uncoated ZnO NS (a), G_{110}-ZnO NS (b) and G_{350}-ZnO NS (c).
2. XRDs pattern of the annealed ZnO-NS without C-coating deposited onto Pt-coated SS. Miller indexes refer to the wurtzite-type ZnO peaks, whereas the contribution due to the substrate are indicated with diamond-shaped symbols (Pt), triangles (SS) and stars (sample holder).

3. Cyclic voltammograms (five cycles) of anode based on ZnO nanosheets film at 0.1 mV s^{-1} and room temperature: a) pristine ZnO nanosheets; b) ZnO nanosheets coated with a 110Å-thick layer of graphite; c) ZnO nanosheets coated with a 350Å-thick layer of graphite. The star indicates the first scan.
4. Galvanostatic charge-discharge curves (a-c) and differential capacities vs. voltage (d-f) of ZnO nanosheets, pristine and coated with layers of graphite with different thickness: 110Å and 350Å. The applied current was 1 Ag^{-1}.
5. Cycling performances of films grown of Pt-SS substrates based on ZnO nanosheets, pristine (circles) and coated with layers of graphite with different thickness: 110Å (squares) 350Å (triangles). Filled symbols: discharge. Open symbols: charge.
6. Coulombic efficiency of films grown of Pt-SS substrates based on ZnO nanosheets, pristine (circles) and coated with layers of graphite with different thickness: 110Å (squares) 350Å (triangles). The wave-like oscillations are due to the changes of ambient temperature.
7. SEM micrographs (Mag. 200kx) of uncoated ZnO NS (a), G_{110}-ZnO NS (b) and G_{350}-ZnO NS (c), collected after the 100 galvanostatic cycles at 1 Ag^{-1} and room temperature.

Anode	***Capacity (mA h^{-1} g^{-1})***	***Current Density (A g^{-1})***	***Cycle Number***	***Reference***
ZnO NS	400	1	100th	This work

ZnO-Graphite (G_{350}-ZnO NS)	600	1	100th	This work
ZnO-GO (NS)	360	0	200th	[21]
ZnO-C (NR)	360	0.75*	30th	[23]
ZnO (NS)	400	0.5	100th	[19]
ZnO (NR)	480	0.5	100th	[32]
ZnO bramble-like	392	0.8	10th	[14]
ZnO niddle-like	240	0.8	10th	[14]
ZnO dandelion-like	310	0.1 mA cm^{-2}	40th	[10]

Table 1: Electrochemical performance comparison of nanostructured anodes based on ZnO arrays for lithium batteries. *Value estimated from the C Rate [23].

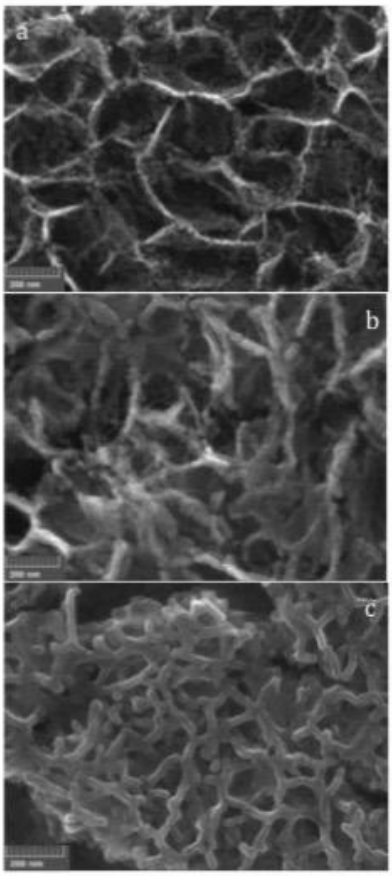

Figure 1

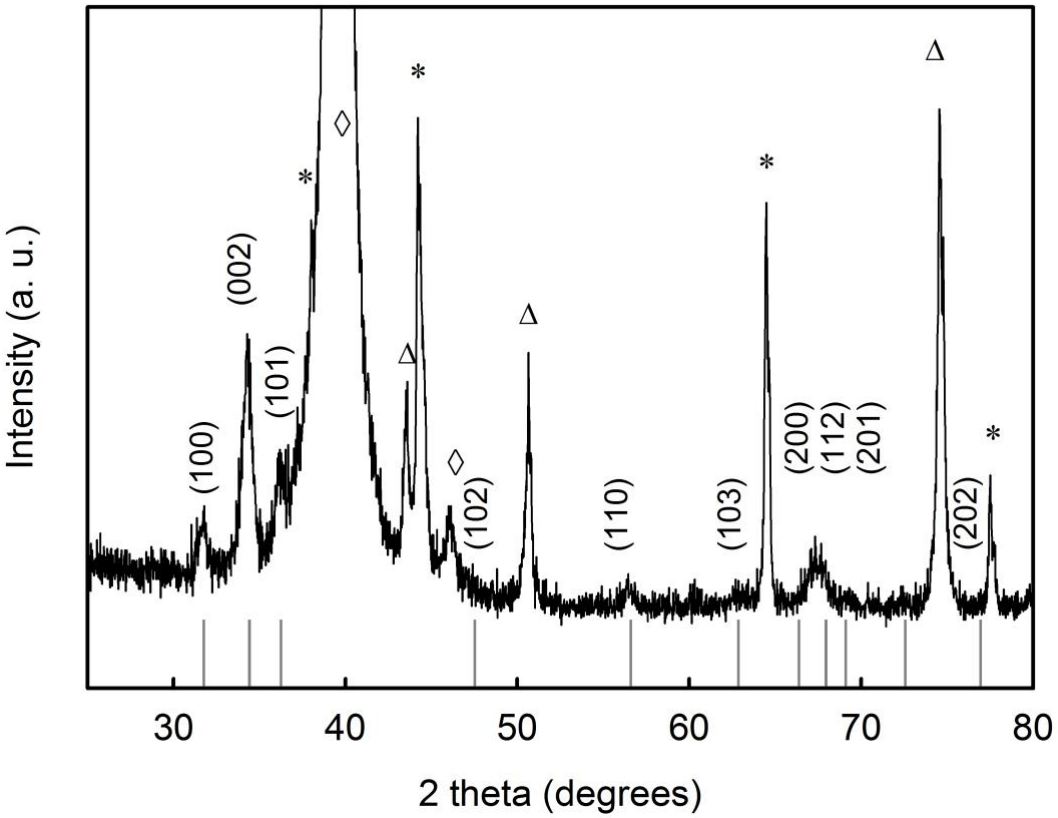
Intensity (a. u.)
2 theta (degrees)
30
40
50
60
70
80
(100)
(002)
(101)
(102)
(110)
(103)
(200)
(112)
(201)
(202)
*
◊
Δ

Figure 2

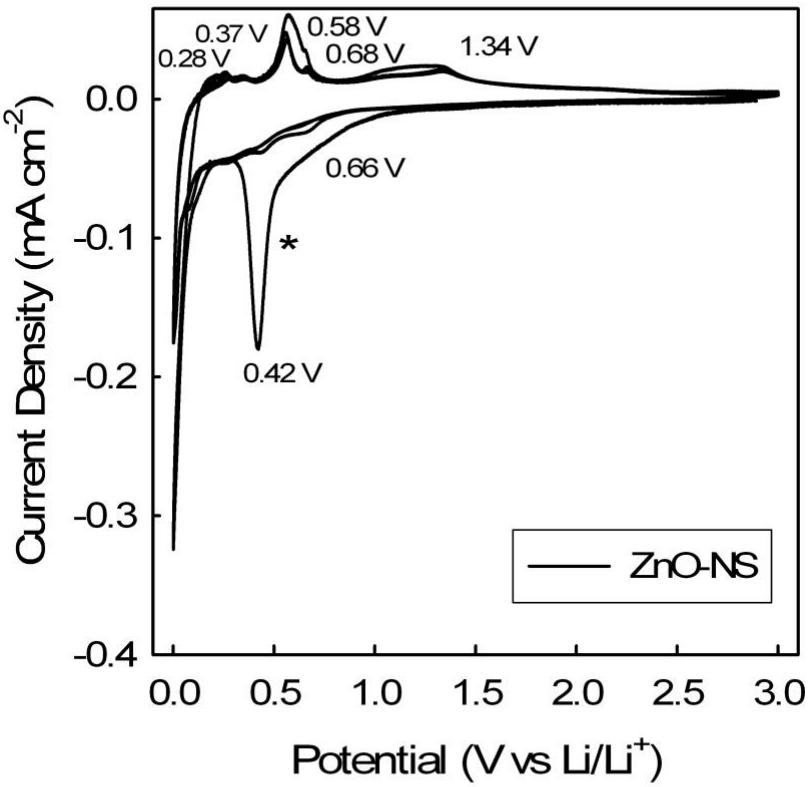
0.37 V
0.58 V
0.28 V
0.68 V
1.34 V
0.66 V
*
0.42 V
ZnO-NS
Current Density (mA cm-2)
Potential (V vs Li/Li+)
0.0
-0.1
-0.2
-0.3
-0.4
0.5
1.0
1.5
2.0
2.5
3.0

Figure 3a

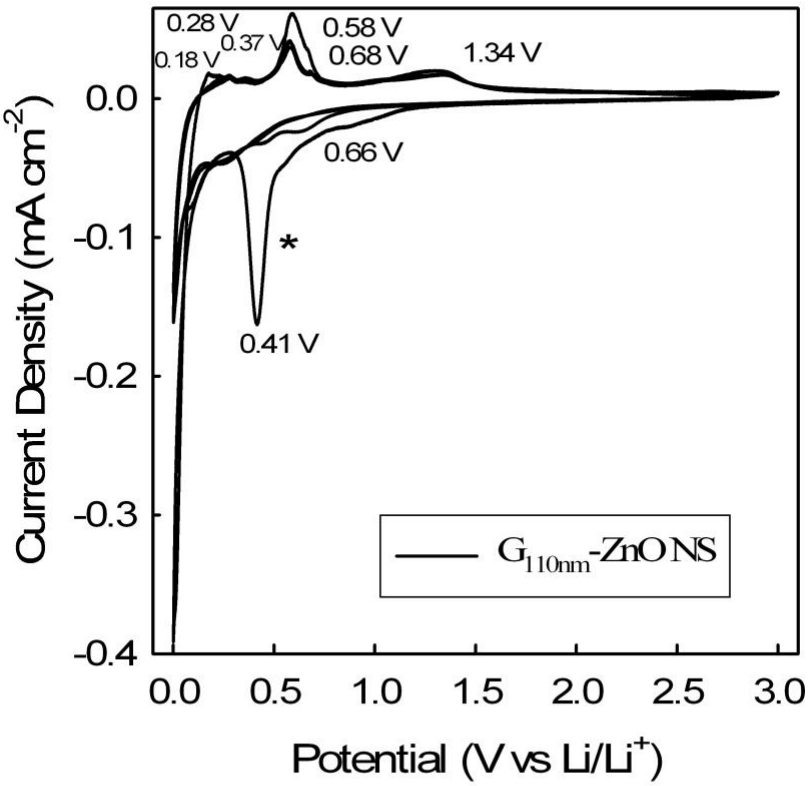
0.28 V
0.37 V
0.18 V
0.58 V
0.68 V
1.34 V
0.66 V
*
0.41 V
G110nm-ZnONS
Current Density (mA cm-2)
Potential (V vs Li/Li+)
0.0
-0.1
-0.2
-0.3
-0.4
0.5
1.0
1.5
2.0
2.5
3.0

Figure 3b

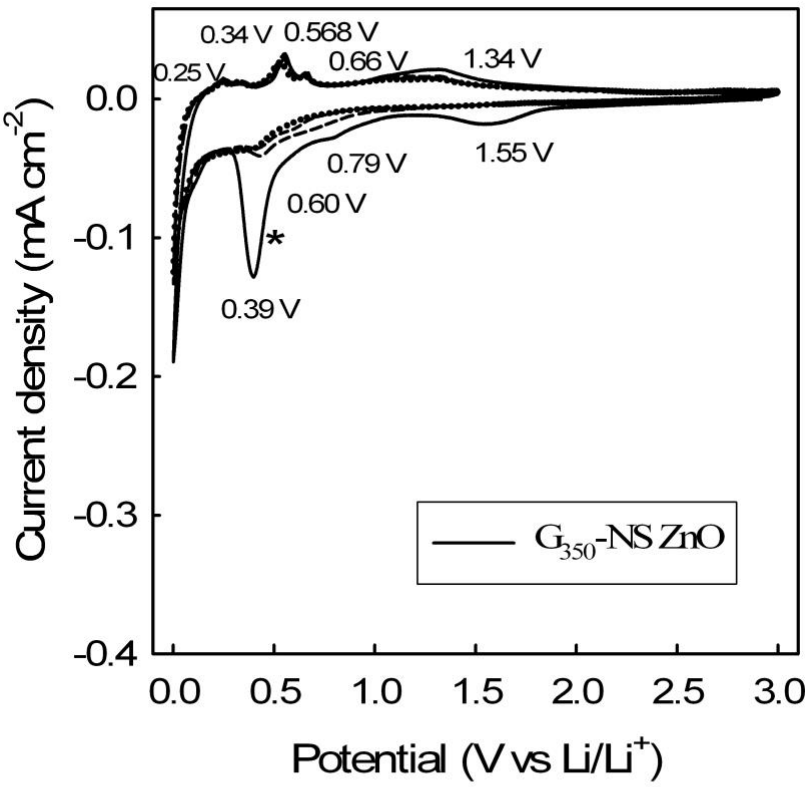
0.34 V
0.568 V
0.25 V
0.66 V
1.34 V
0.79 V
1.55 V
0.60 V
*
0.39 V
G350-NS ZnO
Current density (mA cm-2)
Potential (V vs Li/Li+)
0.0
-0.1
-0.2
-0.3
-0.4
0.5
1.0
1.5
2.0
2.5
3.0

Figure 3c

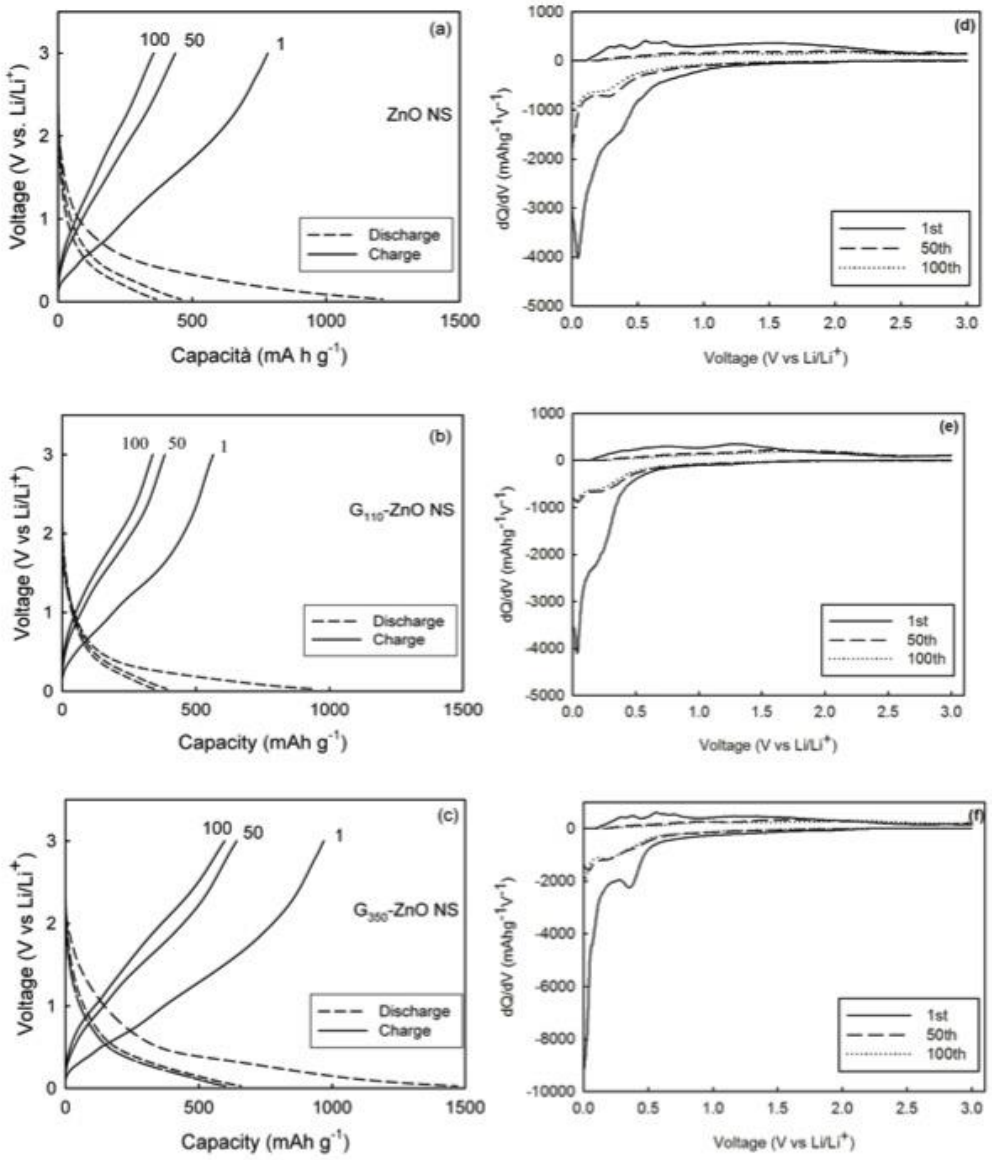
(a)
ZnO NS
100
50
1
Discharge
Charge
Voltage (V vs. Li/Li+)
Capacità (mA h g-1)
(d)
1st
50th
100th
dQ/dV (mAhg-1V-1)
Voltage (V vs Li/Li+)
(b)
G110-ZnO NS
Capacity (mAh g-1)
(e)
(c)
G350-ZnO NS
(f)

Figure 4

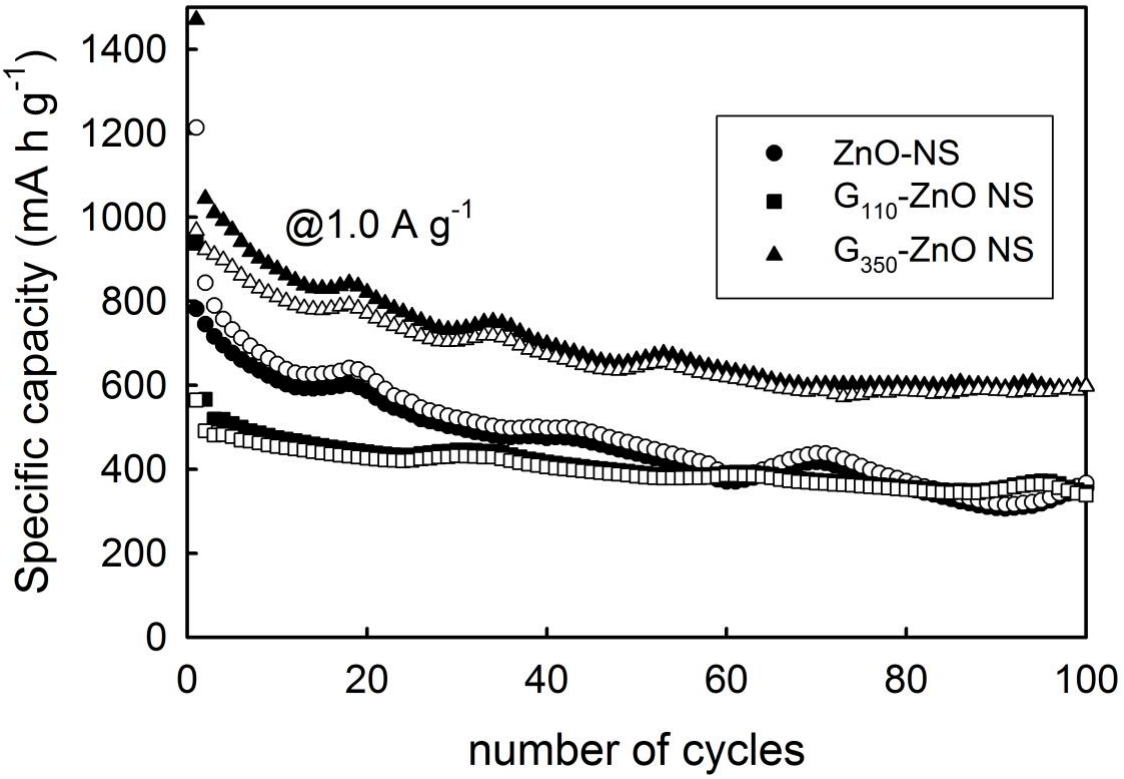
Specific capacity (mA h g-1)
1400
1200
1000
800
600
400
200
0
0
20
40
60
80
100
number of cycles
@1.0 A g-1
ZnO-NS
G110-ZnO NS
G350-ZnO NS

Figure 5

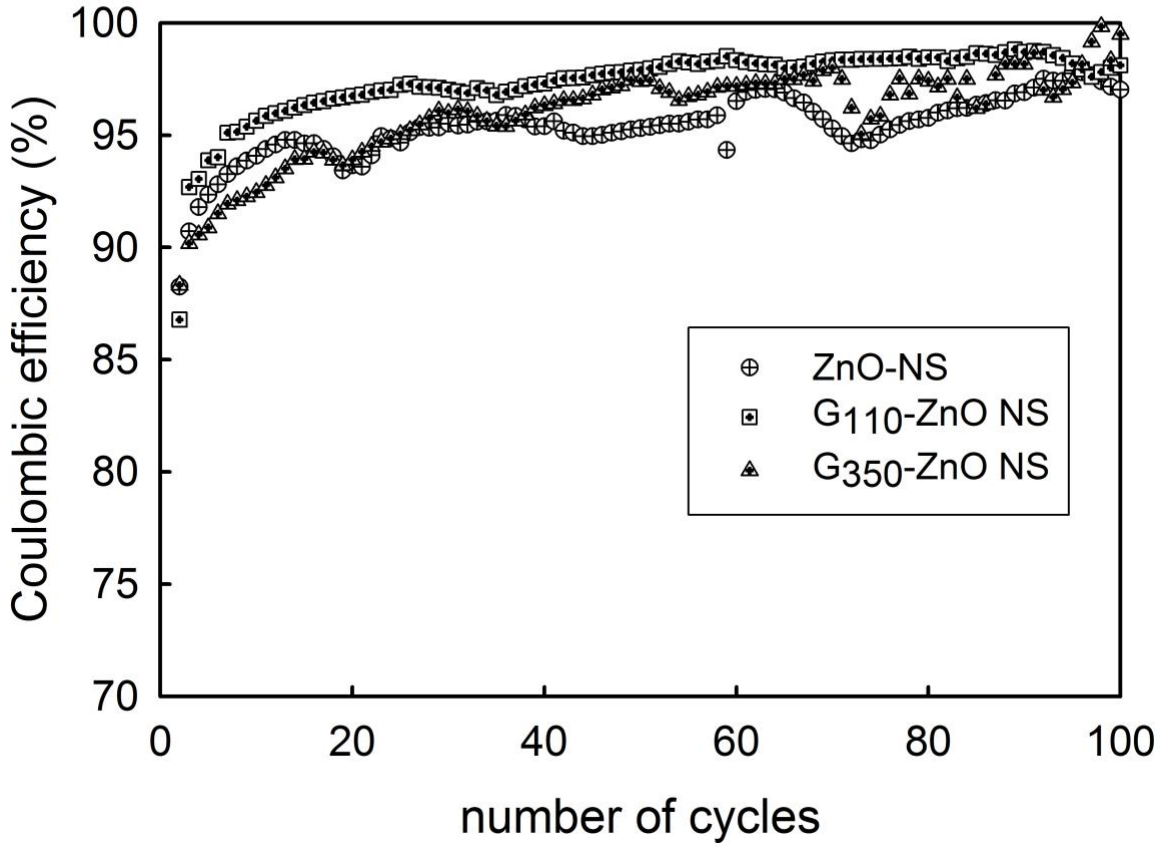
Coulombic efficiency (%)
100
95
90
85
80
75
70
0
20
40
60
80
100
number of cycles
ZnO-NS
G110-ZnO NS
G350-ZnO NS

Figure 6

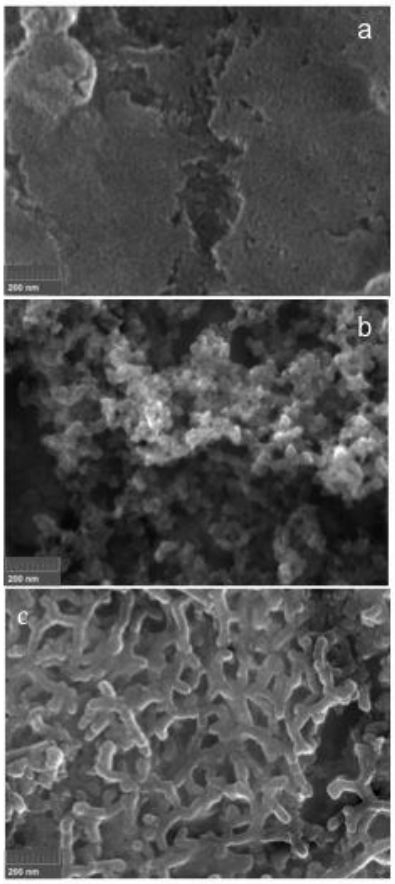

Figure 7